Trajectory Optimisation for Increased Stability of Mobile Robots Operating in Uneven Terrains

Chistoph Beck
University of Karlsruhe
Faculty of Mechanical Engineering
Germany
Email: christoph.beck@student.kit.edu

Jaime Valls Miró and Gamini Dissanayake
Faculty of Engineering and IT
University of Technology Sydney (UTS)
NSW 2007, Australia
Email: javalls,gdissa@eng.uts.edu.au

***Abstract*—A mechanism capable of enhancing the safety of paths followed by mobile robots which significantly modify their mass distribution while operating in uneven terrains is presented. This is the case, for instance, of kinematically reconfigurable platforms or robots equipped with manipulator arms. For a given path, a trajectory optimiser that finds suitably "safer" paths in terms of tip-over prevention and equal force distribution over the supporting contact points is proposed. Other kinematic considerations such as operating within given nominal joint positions or low energy motions can also be exploited to improve system stability while being deployed in specific domains such as security, rescue, etc. Simulation results of the proposed optimised motion planner for an iRobot Explorer tracked vehicle are presented. They are also compared with a non-optimised planners to show the validity of the approach.**

I. Introduction

The application domain of mobile robots is rather vast nowadays. While some robots are designed to be deployed in well-known, flat, homogeneous terrains, others have to deal with rough terrains and many uncertainties. Such is the case of planetary exploration rovers, agriculture, mining or rescue robots. In these cases, terrain parameters (i.e. shape, inclination or soil properties) have a strong influence on the robot's ability to perform as planned. For the specific case of reconfigurable robots operating in these conditions, their kinematic configuration also play a crucial factor in the interaction between vehicle and terrain to be able to successfully accomplish their given missions. For these cases, the ability to actively assume safer poses that reduce potential instabilities, such as those leading to vehicle tip-over, is a desirable feature.

There have been a number of recent publications that address the issue of stability in mobile robots. Some research has focused on the analysis of the robot's Centre of Gravity (CoG) to find suitable controls to cope with specific scenarios like overcoming obstacles and small ditches [1] [2] or climbing stairs [3]. Shoval [4] examined a multi tracked robot on a steep slope to determine boundaries for the CoG and came up with a strategy to traverse a given slope. Rey and Papadopoulos [5] introduced a stability margin measure to estimate the predicted time until tip-over for large mobile manipulator robots, such as forestry vehicles. They also recommended stabilising steps by using certain actuators. A real-time rollover protection strategy was developed by Inoue et al. [6]. It was based on whole-body touch sensors that are embedded in the tracks of the robot and an energy stability margin that serves as an indicator for jeopardised robot configurations. Stabilising actions to protect the robot from rolling over based upon empirical flipper movement were also proposed.

More general approaches for the stability control of reconfigurable mobile robots which also take into account other constraints such as traction optimisation were developed by Dubowsky et al. [7], and very recently by Bidaud et al. [8]. In both works, the Force-Angle Stability Margin (FASM) originally introduced by Papodopoulos and Rey in 1996 [9] was used. Dubowsky et al. defined a performance index that considered the stability measure for each potential tip-over axis and the nominal values of the joints. The minimisation of this performance index provided the most favourable configuration of the robot. Bidaud et al. combined the stability measure with an artificial potential field to obtain the demanded actuator values. Both works are however inadequate for certain robot configurations, or in general for robots with low CoG. The stability measure employed considers the angle between the vector through CoG and tip-over axis and the vector of the resulting force through the CoG. This may be sufficient for a robot with relatively high and not significantly changing CoG, but is not representative for the actual stability in many other cases, as will be further discussed in Section II-A.

In this study, a stability measure is used that includes the horizontal distance between CoG and tip-over axis, also proposed by Papadopoulos and Rey in a later article [10], thereby providing a more reliable measure for the stability about each tip-over axis. Based on this analysis, a novel trajectory optimiser is proposed to enhance the safe traversability of a given path over irregular terrain, assumed here to serve other navigational purposes (e.g. exploration, SLAM, etc). A proposed cost function is defined around the stability margin to address four key objectives:

1) prevention of tip-over and operation within certain safety limits, the key
2) equal distribution of the resulting forces on the supporting points
3) operating within nominal joint positions
4) low energy consumption

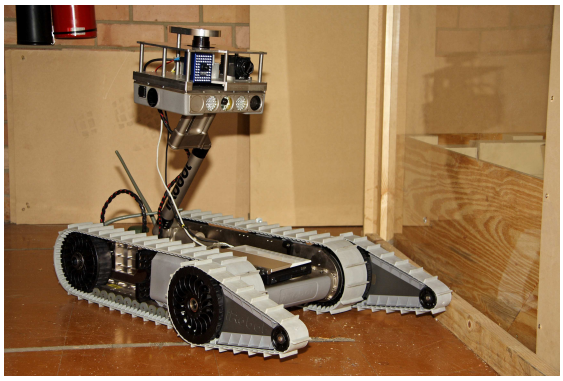

Fig. 1. The iRobot Packbot tracked robot fitted with the Explorer arm, and an additional sensor payload mounted on the pan and tilt unit.

In this work, the proposed planning strategy is illustrated with the quasi-static model of the multi-tracked iRobot PackBot platform, mounted with an arm and pan and tilt unit, and an additional sensor head on top of it, as depicted in Figure 1.

II. Stability Measure

Stability Margins have been playing a decisive role in the history of walking robots. McGhee and Frank [11] examined the static stability of a walking vehicle for the first time in 1968. They claimed that the vehicle is stable if the horizontal projection of the CoG lies within the support polygon that is formed by the contact points between vehicle and ground. The corresponding Static Stability Margin (SSM) was defined as the smallest distance between the projected CoG and the edge of the polygon. The SSM was later adapted to uneven terrain and slightly modified to reduce the complexity of calculation [12]. The main disadvantage of these purely projective-based approaches is the insensitiveness to the height of the CoG. The Energy Stability Margin (ESM), introduced by Messuri [13], solved this problem by determining the potential energy that is needed to tumble the vehicle and represents a reliable static stability margin. Hirose et al. [14] finally normalised this measure to obtain a more general and meaningful measure of stability.

Dynamic effects introduced through accelerations of the whole vehicle or certain components were firstly addressed by Orin [15]. The author presented an extension of the SSM where the CoG was projected onto the support polygon along the vector of the resulting force through the CoG. The resulting forces include dynamic effects, and the system is stable as long as the projection lies within the polygon. Other works refer to this point as the Zero Moment Point (ZMP) [16] where the resulting moment due to reaction forces and moments vanishes. Lin and Song [17] proposed the momentum-based Dynamic Stability Measure (DSM). It is equal to the smallest of all moments about the edges of the support polygon that prevents the vehicle from tipping over, calculated on the basis of reaction forces and moments. Based on the ESM, Garcia and Santos [18] developed the Normalised Dynamic Energy Stability Margin that covers all dynamic effects but is computationally rather expensive. The Force-Angle stability margin (FASM), proposed by Papadopoulos and Rey [10], also covers dynamical changes in the robot configuration and is subject to external forces and moments, but has a more simplistic geometric interpretation and thus can be more easily computed, therefore being a more suitable stability measure for mobile robots/manipulators, and is the metric employed in this work. It was introduced in two different versions, which are briefly reviewed in the next Section to better understand the influence of the CoG's height in the performance of the measure for platforms that can significantly reposition their centre of mass to improve stability in uneven terrains.

A. The Force-Angle Stability Margin (FASM)

The original FASM measure, hereby refered to as β, was introduced by Papadopoulos and Rey in 1996 [9], is given by

$$\beta = min(\theta_i \|\mathbf{f_i}\|) \tag{1}$$

where $\mathbf{f_i}$ is the net force (including all static and dynamic forces, as well as moments) contributing to a potential roll-over about a particular tip-over axis $\mathbf{a_i}$. The tip-over axes $\mathbf{a_i}$ are given as the lines between m arbitrary supporting points $\mathbf{p_i}, i = \{1, .., m\}$

$$\mathbf{a_i} = \mathbf{p_{i+1}} - \mathbf{p_i}, i = \{1, .., m-1\} \tag{2}$$

$$\mathbf{a_m} = \mathbf{p_1} - \mathbf{p_m} \tag{3}$$

θ_i is the angle between $\mathbf{f_i}$ and the tip-over axis normal through the tip-over axis and the CoG. Figure 2 illustrates these parameters in a two dimensional example, where $\mathbf{a_1}$ and $\mathbf{a_3}$ are perpendicular to the paper representing the tip-over axes through $\mathbf{p_1}/\mathbf{p_2}$ and $\mathbf{p_3}/\mathbf{p_4}$ respectively.

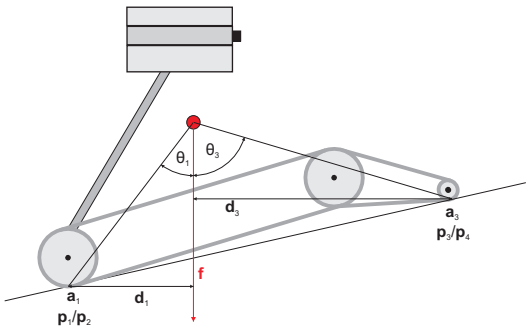

Fig. 2. Example FASM in 2D.

The revised version of FASM was published in 2000 [10] and besides $\mathbf{f_i}$ and θ_i also included $\mathbf{d_i}$, the distance between $\mathbf{a_i}$ and $\mathbf{f_i}$ as

$$\beta = min(\theta_i \ \|\mathbf{d_i}\| \ \|\mathbf{f_i}\|) \tag{4}$$

This enables the metric to become sensitive to varying heights of the CoG. The greater the value of the stability measure β_i, the more stable the vehicle becomes in terms

of tipping over about the given axis. Negative values of the measure indicate an occurring tip-over instability.

The tip-over axis normal $\mathbf{l_i}$ that intersects the CoG is given by

$$\mathbf{l_i} = (I - \hat{\mathbf{a}}_\mathbf{i}\hat{\mathbf{a}}_\mathbf{i}^\mathbf{T})(\mathbf{p_{i+1}} - \mathbf{p_{CoG}}) \tag{5}$$

where $\hat{\mathbf{a}}_\mathbf{i}$ is the normalised vector of $\mathbf{a_i}$, $\mathbf{p_{CoG}}$ is the position of the CoG and I is the 3×3 identity matrix.

Given $\mathbf{f_r}$, the net force acting on the CoG which includes gravitational, external and inertial forces, and $\mathbf{n_r}$, the net moment encompassing all external and inertial moments about the CoG axis, the effective net force $\mathbf{f_i}$ that contributes to a potential tip-over about one specific axis $\mathbf{a_i}$ can be determined by

$$\mathbf{f_i} = (I - \hat{\mathbf{a}}_\mathbf{i}\hat{\mathbf{a}}_\mathbf{i}^\mathbf{T})\mathbf{f_r} + \frac{\hat{\mathbf{l}}_\mathbf{i} \times ((\hat{\mathbf{a}}_\mathbf{i}\hat{\mathbf{a}}_\mathbf{i}^\mathbf{T})\mathbf{n_r})}{\|\mathbf{l_i}\|} \tag{6}$$

The first term considers the part of the net force perpendicular to the tip-over axis. The second term considers the moment that participates about the tip-over axis, converted into an equivalent force couple, where one member of the couple passes through the CoG and thus can be added to the net force, whereas the other member passes through the tip-over axis and hence does not contribute to $\mathbf{f_i}$.

The angle θ_i for each tip-over axis can then be computed by

$$\theta_i = \sigma_i \cos^{-1}(\hat{\mathbf{f}}_\mathbf{i}\hat{\mathbf{l}}_\mathbf{i}) \tag{7}$$

where

$$\sigma_i = \begin{cases} +1 & (\hat{\mathbf{f}}_\mathbf{i} \times \hat{\mathbf{l}}_\mathbf{i})\hat{\mathbf{a}}_\mathbf{i} > 0 \\ -1 & \text{otherwise} \end{cases} \tag{8}$$

The new FASM also requires the shortest distance $\mathbf{d_i}$ between $\mathbf{a_i}$ and $\mathbf{f_i}$, which can be obtained by adding the projection of $\mathbf{l_i}$ on $\mathbf{f_i}$ to negative $\mathbf{l_i}$, i.e.

$$\mathbf{d_i} = -\mathbf{l_i} + (\mathbf{l_i^T}\,\hat{\mathbf{f}}_\mathbf{i})\,\hat{\mathbf{f}}_\mathbf{i} \tag{9}$$

For more details on these derivations, the reader is refered to [10].

A stability analysis based on the old FASM is not adequate for the universal application to mobile robots. Consider for example the scenario shown in Figure 3 with the PackBot robot examined during the testing of this work. The CoG is naturally rather low, yet the arm and payload position play a significant role in the stability of this robot pose. The two arm positions illustrated in the example result in CoG positions that span one line with the tip-over axis and hence share the same angle $\theta = \theta'$. However, it is obvious that the vehicle becomes more unstable with a decreasing distance between the CoG and tip-over axis. Therefore, the FASM metric defined by (4) is used as the stability measure in this work and is the basis for the trajectory optimiser proposed in this work.

B. Normalisation

It is advisable to normalise the obtained stability measure for a most stable configuration. Normalisation facilitates the general interpretation of the stability measure independently of the vehicle type and permits meaningful comparisons of

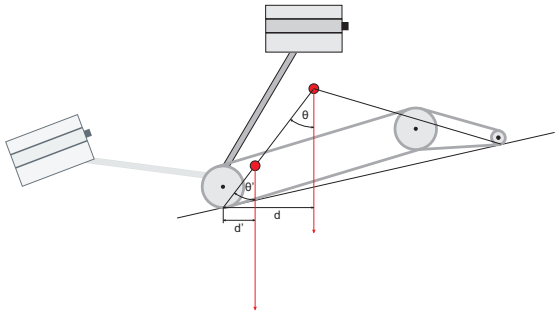

Fig. 3. Comparison of both version of the FASM.

the same control algorithms based on the stability measures in different vehicles. The normalised measure $\hat{\beta}_i$ is given by:

$$\hat{\beta}_i = \frac{\beta_i}{\beta_{norm}} \tag{10}$$

where β_{norm} is chosen to be the stability measure for the vehicle in horizontal position with arms in a stable, folded configuration.

III. Performance Index

A performance index designed around the stability measure is proposed as a basis for a motion planner capable of generating optimised feasible trajectories analytically guaranteed to be reliably stable for a given terrain-following path (not addressed in this work), with the ultimate objective of autonomous robot operation in mind. Automatic safe planning is also a desirable addition for remote controlled robot scenarios as it enables the operator to focus on the main platform driving commands, or other application-dependent tasks such as searching for victims or indicating broad directions for exploration, while the kino-dynamic stability of the vehicle for the safe operation of the vehicle is automatically secured.

While tip-over prevention is the key objective for stability control, other objectives like nominal values of certain robot links, the equal distribution of reaction forces and consequent optimisation of traction, or the minimisation of energy expenditure are also addressed. A performance index C that considers these criteria is proposed in this work as

$$\begin{aligned} C \;=\; & \sum_{i=1}^{n} K_{Ai}C_{Ai} + \sum_{k=1}^{p} K_{Bk}C_{Bk} + \\ & \sum_{j=1}^{m} K_{Cj}C_{Cj} + \sum_{j=1}^{m} K_{Dj}C_{Dj} \end{aligned} \tag{11}$$

where n is the number of tip-over axes (four in this work), p is the number of coupled axes (as described in Section III-B) and m is the number of all internal joints. K_{Ai}, K_{Bk}, K_{Cj} and K_{Dj} are gain factors for the corresponding sub-criteria parameters C_{Ai} (tip-over stability), C_{Bk} (equal force distribution), C_{Cj} (nominal joint positions) and C_{Cj} (energy consumption), hence permitting a customisation of the objective based on

the given application (better traction, less motion, etc). The minimisation of (11) will lead to the new demanded joint positions Φ_j to be followed by the robot.

The various criteria formulated in (11) are defined in more detail in the following sections.

A. Tip-over Stability

C_A aims at securing the robot's stability in order to prevent a tip-over in any configuration. It is defined as

$$C_A = \begin{cases} \infty & \beta_i < \beta_{safe} \\ (\frac{1}{\beta_i - \beta_{safe}} - \frac{1}{\beta_{min} - \beta_{safe}})^2 & \beta_{safe} \geq \beta_i \geq \beta_{min} \\ 0 & \beta_i > \beta_{min} \end{cases} \tag{12}$$

where β_i is the stability measure for tip-over axis i as defined by (10), $\beta_{min} > \beta_{safe}$, and β_{safe} represents a safety limit to compensate for model uncertainties, disturbances and unexpected events. Stability measures below β_{safe} are not tolerated and the term tends to infinity. Values greater than β_{min} will not contribute to the performance index, thus preventing an unnecessary tradeoff between tip-over stability and other objectives.

B. Equal Force Distribution

This term describes how uniformly distributed the reaction forces acting normal to the terrain are on opposite ground contact pairs. A reward of reduced discrepancies contributes to optimised traction and minimisation of unwanted effects like self-digging of the tracks. It is a linear term described by

$$C_{Bk} = |\beta_k - \beta_{k\prime}| \tag{13}$$

where β_k and $\beta_{k\prime}$ are the stability measure of opposing tip-over axis.

C. Nominal Joint Positions

Depending on the application, nominal positions need to be considered in order to bring the sensors into suitable positions, e.g. maintaining ground clearance or increasing situational awareness. This term is an indication of such variability, and is defined as

$$C_{Cj} = (\Phi_j - \Phi_{nom,j})^2 \tag{14}$$

where Φ_j is the position of the jth joint and $\Phi_{nom,j}$ is its nominal position.

D. Energy Consumption

The term is intended to restrict slight link motions between two consecutive way-points and aims at leaving them in their current position in as much as it is feasible. For battery-operated mobile robots energy is a critical resource, thus decreasing energy consumption is particularly relevant, even more so when operating in rough terrains or areas of difficult access. This term is defined by

$$C_{D,j} = \begin{cases} 0 & \Delta\Phi_j < \Delta\Phi_{min} \\ \frac{\Delta\Phi_j - \Delta\Phi_{min}}{\Delta\Phi_{max} - \Delta\Phi_{min}} & \Delta\Phi_{min} \geq \Delta\Phi_j \geq \Delta\Phi_{max} \\ 1 & \Delta\Phi_j > \Delta\Phi_{max} \end{cases} \tag{15}$$

with $\Delta\Phi_{min} < \Delta\Phi_{max}$ and $\Delta\Phi_j$ is the difference between the current and the new demanded position of the jth joint. $\Delta\Phi_{min}$ and $\Delta\Phi_{max}$ are thresholds whose value determine the hysteresis response.

IV. Application Example

The proposed trajectory optimiser is demonstrated with a multi-tracked rescue robot, the iRobot Packbot shown in Figure 1. The robot consists of a skid-steer tank-like vehicle base, equipped with two front flippers that enable the robot to traverse obstacles and rough terrain. The robot arm has three DoF's (shoulder and a pan and tilt unit at the end of it), and has also been fitted with an additional payload in the form of a sensor head mounted on top of the pan and tilt unit. The vehicle base, arm and flipper have the greatest impact on the CoG and are therefore the controllable links considered by the stability optimiser. The orientation of the sensor head is also controllable but the induced static and dynamic effects in the calculations can be neglected in comparison. The results hereby presented are restricted to simulation work while the algorithms are being ported to the real platform.

A. Robot Model

Three coordinate systems are used to model the robot in a convenient way. These are referred to as R (robot), S (slope) and W (world). R represents the local frame, where x_R is the robot's roll axis, y_R the pitch axis and z_R the direction normal to the platform. The robot configuration and its CoG are expressed in reference to R. S is used to represent the orientation of the terrain, which is regarded as a virtual slope, spanned by the contract points between robot and terrain. W is the reference frame with its z-axis opposing the gravitational force. The path the robot must follow is therefore expressed as 3D poses with translations in W and orientations provided by the terrain slope in S at those points. The relevant relationship between the orientation of the various frames used to calculate the CoG of the robot at the given point is given by the rotation matrices ${}^R_S R$ and ${}^S_W R$.

The CoG obtained in the robot frame is given by:

$${}^R CoG = \frac{\sum_{i=1}^{n} p_{mi} m_i}{m_{tot}} \tag{16}$$

where $p_{m,i}$ is the position of the lumped mass m_i and m_{tot} is the total robot mass. In this work the platform is assumed to make contact with the surface at four equidistant points. They are assumed to be lengthwise symmetrical, depicting two possible convex quadrilateral contact surface as shown in Figure 4. Two contact points are always fixed at the robot base rear sprocket. As flippers operate simultaneously on the Packbot, the other two contacts are chosen based on the flipper pose. When the flippers touch the ground the front contact is at the flipper's front sprockets, defining an isosceles trapezoid as depicted in Figure 4b. When the flippers do not interact with the terrain, the front contact is assumed to be at the robot base front sprockets, thus describing a rectangular area, as shown in Figure 4a. The connecting lines between the ground contacts represent the tip-over axes $a_i, i = \{1, .., 4\}$.

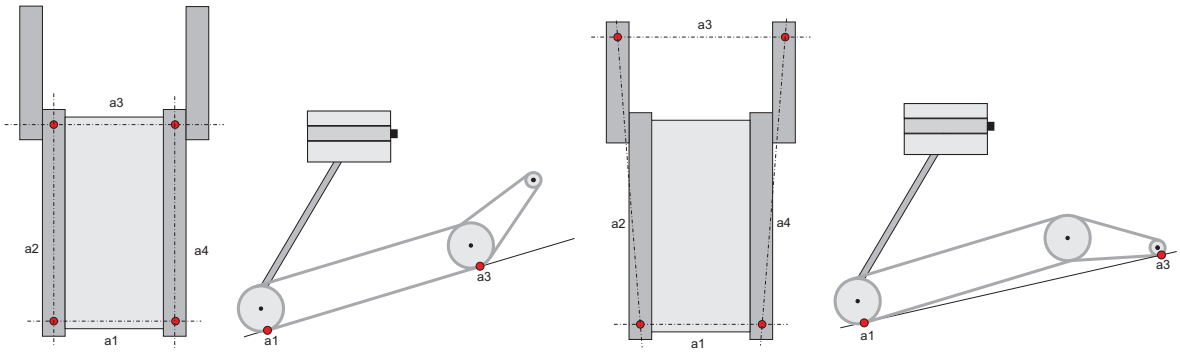

(a) Flippers up contact points (b) Flippers down contact points

Fig. 4. Surfaces defined by the contact points used to calculate the robot Centre of Gravity.

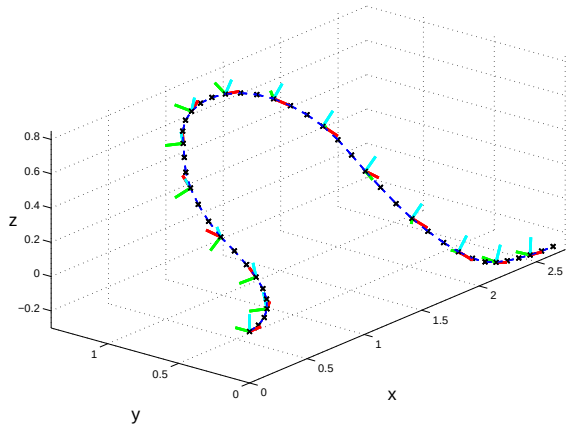

Fig. 5. Robot path in 3D

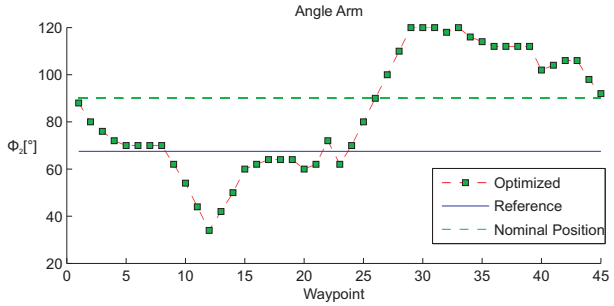

Fig. 6. Optimised and reference arm trajectory.

B. Simulation Results and Analysis

The simulation has been conducted for quasi-static conditions. While the formulation allows for dynamic effects to be readily incorporated, they are neglected in this work and only gravitational forces are considered for now. The optimisation has been carried out for the example path illustrated by the uniformly spaced way-points in Figure 5, assumed to be given by some external three-dimensional path planner. The resulting arm and flipper trajectory has been compared with a realistic scenario where flippers and arm are locked in $0°$ and $67.5°$ (mid-height) respectively. These values are reasonable for manual operation of the robot without considering arm and flipper adjustments on the fly.

The stability measures are evaluated based on (4) and normalised for the left tip-over axis, which holds the smallest stability measure for the robot's home configuration (the weight of the robot is almost symmetrically distributed except for the weight of the battery which is concentrated on one side). The home configuration is defined on a level surface with the flippers in a $180°$ position parallel to the robot's base and the head in its lowest position ($0°$).

The gain factors and threshold values used in calculating (11) have been chosen according to the following assumptions: tip-over stability about all tip-over axes is assessed equally, which leads to one common weight K_A. The threshold value β_{min} is set to 0.5, hence initiating tip-over preventing action if a stability measure falls below 50% of the stability margin gained in the home configuration. A "safety margin" of $\beta_{safe} = 0.2$ has been empirically found to be reasonable to compensate for dynamic effects and unmodelled uncertainties. For an equal force distribution, opposing tip-over axes (back-front and left-right) are examined and assessed with the gains K_{B1} and K_{B2}. The preferred nominal joint positions are those that can provide high exposition of the sensor head in order to guarantee improved visual feedback from the camera sensors mounted on the head unit back to the remote operator. The nominal value of the arm is set to a position of $90°$ in reference to the base and weighted by K_C. Lastly, K_{D1} and K_{D2} are used to assess the position difference of flippers and arm between two consecutive way-points.

Figures 6 and 7 depict the optimised payload arm and flipper trajectories, obtained from an exhaustive search for the minimum cost at each way-point (the actual search algorithm employed is not relevant to the scope of this work). The maxiumum feasible distance between consecutive flipper and arm positions is restricted to $8°$ and $10°$ to benefit the smoothness of the resulting trajectory in conjunction with the energy term. The blue line represents the nominal position of

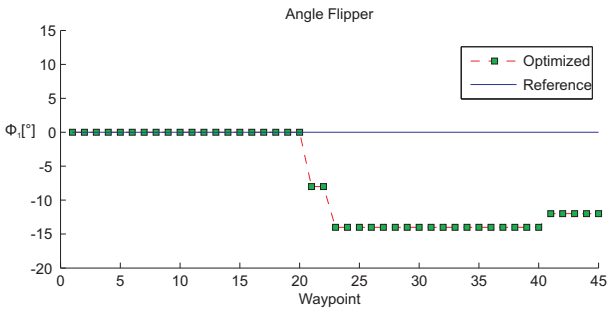

Fig. 7. Optimised and reference flipper trajectory.

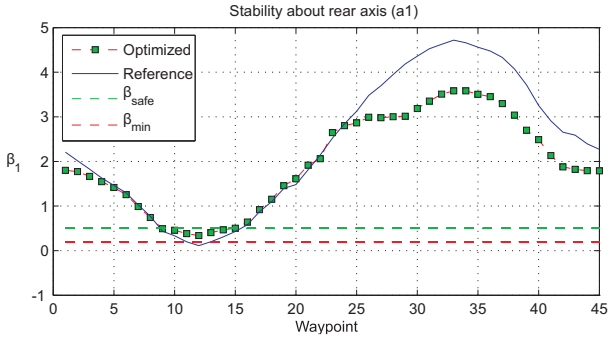

Fig. 8. Stability Margin about back tip-over axis

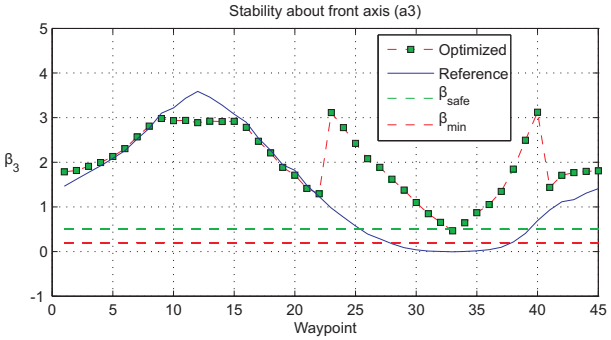

Fig. 9. Stability Margin about front tip-over axis

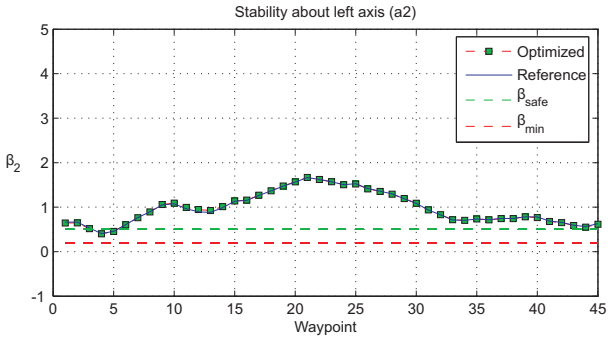

Fig. 10. Stability Margin about left tip-over axis

$90°$. It can be observed how the difference between nominal and actual arm joint positions can vary by as much as about $45°$. This relatively large discrepance is enforced by the need for a low CoG for certain inclination so as to guarantee a stable foothold.

The resulting stability measures about all tip-over axes are shown in Figures 8 to 11. It can be seen how all measures are greater then the chosen threshold of $\beta_{safe} = 0.2$. The robot operates in the allowed stability area and tip-over is prevented. In comparison to this, the stability measures for the comparative trajectory with fixed arm and flipper positions are illustrated by the blue lines. It can be observed how at way-point 12 the robot operates inside the critical zone about the rear axis, whereas the stability measure for the front axis reaches zero at way-point 32 and a tip-over would occur at this point. It is also apparent how when the terrain becomes flatter and less challenging in terms of tip-over (areas where the minimum stability values β_{min} are maintained), the importance of the alternative criteria becomes more apparent. As a result, the head stays primarily in the more upright positions (nominal value) and actuator motions and force distributions are traded-off.

C. Performance Index Analysis

In order to analytically comprehend the effects of the weighing factors proposed in (11), a range of values have been studied during the optimisation of the given path. The results of these tests for the various criteria are collected in Tables 12a to 12d. During the testing of each gain, the medium values for the other coefficients have been used.

In Table 12a, the minimum value of the stability measure β_i during the whole simulation is proposed as a representative evaluation criteria for the stability coefficient analysis. It is shown how low gains K_A result in low stability margins, virtually on the safety threshold β_{safe}. A high gain, on the contrary, keeps a comfortable safety buffer.

Equal force distribution is assessed by the difference between forces acting normal to the slope in coupled axis. For simplicity, only the difference between the rear and front axis is considered and normalised over their sum to facilitate representative comparison between different inclinations. Both the worst-case difference $max(\Delta F)$ and the average $\overline{\Delta F}$ during the whole simulation are shown. Table 12b suggests how a high factor minimises the average variations and also raises the minimum values during the simulation, hence contributing to better overall traction.

Table 12c collects the results of adjusting the nominal position gain K_C. Higher indexes lead to low average deviations $\overline{\Delta\Phi_2}$ between nominal and actual arm position. Maximum deviation $max(\Delta\Phi_2)$ also decreases. On the other hand, a low gain allows for larger deviations from the nominal values.

Finally, results in terms of energy expenditure are displayed in Table 12d, represented by the percentage of the joint motion between two consecutive way-points relative to the maximum feasible distance. For simplicity, only the arm joint is shown. A low factor of K_{D2} leads to higher energy usage of more than 50% over the average values, whereas a higher factor decreases this value significantly, and joint motions are minimised as a result.

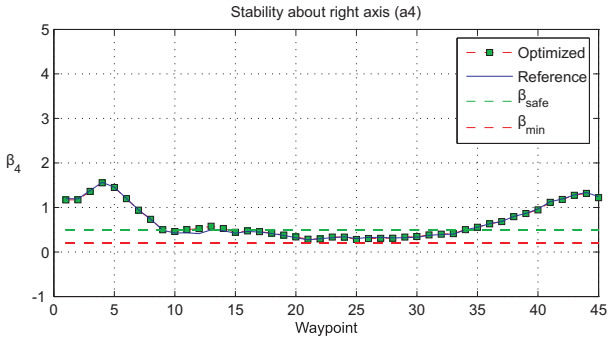

Fig. 11. Stability Margin about right tip-over axis

K_A	β_{min}	tip axis
0.1	0.217	rear
1.1	0.281	right
10.1	0.382	front

(a) Stability

K_{B1}	$\overline{\Delta F}$	$max(\Delta F)$
0.5	0.179	0.44
5.5	0.12	0.303
10.5	0.108	0.268

(b) Force Distribution

K_C	$\overline{\Delta\Phi_2}$	$max(\Delta\Phi_2)$
1.5	42.7	82
15.5	22.9	56
25.5	15	48

(c) Nominal Joint Position

K_{D2}	$\overline{\Delta\Phi_2}/\Delta\Phi_{max}$
0.05	0.57
0.5	0.46
5	0.16

(d) Energy Consumption

Fig. 12. Performace index tables

V. Conclusion and Further Work

A strategy is presented to plan safer trajectories in uneven terrains for robots that can significantly reposition their centre of mass. With the knowledge of the various robot masses involved, the robot kinematics and the terrain (contact points), the Force Angle Stability Measure criterion is innovatively used in conjunction with additional application-dependant objectives such as operating within nominal poses or equi-distribution of traction to accomplish safest possible navigation over challenging, irregular terrains. Results demonstrate marked improvements primarily in tip-over prevention, in particular when compared with more simplistic strategies that do not account for the resulting forces exerted at the robot support points. In this work, robots are assumed to operate in quasi-static conditions. While this is true for robots operating in environments such as rescue or planetary exploration, where the benefits of this strategy are more apparent, disregarding dynamic moments is nevertheless a shortcoming that is currently being addressed. Also, the assumption of four symmetrical support points, while also realistic of the aforementioned deployment scenarios most interesting for the application of this work, is nevertheless currently being lifted.

Acknowledgment

This work is supported by the Australian Research Council (ARC) through its Centre of Excellence programme, and by the New South Wales State Government. The ARC Centre of Excellence for Autonomous Systems (CAS) is a partnership between the University of Technology Sydney, the University of Sydney and the University of New South Wales. Christoph Beck is a visiting research student of CAS from the University of Karlsruhe (Germany).

References

[1] W. Wang, Z. Du, and L. Sun, "Dynamic load effect on tracked robot obstacle performance," in *Proceedings of International Conference on Mechatronics WA1-B-4, Kumamoto, Japan*, 2007.

[2] ——, "Kinematics analysis for obstacle climbing performance of a rescue robot," in *Proceedings of the 2007 IEEE International Conference on Robotics and Biomimetics, Sanya, China*, 2007.

[3] P. Ben-Tzvi, S. Ito, and A. A. Goldenberg, "Autonomous stair climbing with reconfigurable tracked mobile robot," in *ROSE 2007 - IEEE International Workshop on Robotic and Sensors Environments, Ottawa - Canada, 12-13 October 2007*, 2007.

[4] S. Shoval, "Stability of a multi tracked robot traveling over steep slopes," *Proceedings of the IEEE International Conference on Robotics & Automation, New Orleans, LA, USA*, 2004.

[5] D. A. Rey and E. G. Papadoupoulos, "Online automatic tipover prevention for mobile manipulators," *Proceedings of the 1997 IEEE/RSJ International Conference on Intelligent Robots and Systems*, vol. 3, pp. 1273–1278, 1997.

[6] D. Inoue, K. Ohno, S. Nakamura, and S. Tadokoro, "Whole-body touch sensors for tracked mobile robots using force-sensitive chain guides," in *Proceedings of the 2008 IEEE International Workshop on Safety, Security and Rescue Robotics, Sendai, Japan, October 2008*, 2008.

[7] P. Schenker, T. Huntsberger, P. Pirjanian, S. Dubowsky, K. Iagnemma, and V. Sujan, "Rovers for agile, intelligent traverse of challenging terrain," *Proceedings of the 7th International Symposium on Artificial Intelligence, Robotics and Automation in Space, i-SAIRAS, Nara, Japan, May*, 2003.

[8] G. Besseron, C. Grand, F. B. Amar, and P. Bidaud, "Decoupled control of the high mobility robot hylos based on a dynamic stability margin," *IEEE/RSJ International Conference on Intelligent Robots and Systems, Nice, France, September 22-23*, 2008.

[9] D. A. Rey and E. G. Papadoupoulos, "A new measure of tipover stability margin for mobile manipulators," *Proceedings of the IEEE International Conference on Robotics and Automation, Minneapolis, Minnesota, April*, 1996.

[10] ——, "The force angle measure of tipover stability margin for mobile manipulatiors," *Vehicle System Dynamics*, vol. 33, pp. 29–48, 2000.

[11] R. McGhee and A. Frank, "On the stability properties of quadruped creeping gaits," *Mathematical Bioscience 3*, vol. 3, pp. 331–351, 1968.

[12] R. McGhee and G. Iswandhi, "Adaptive locomotion of a multilegged robot over rough terrain," *Systems, Man and Cybernetics*, vol. 4, pp. 176–182, 1979.

[13] D. A. Messuri and C. Klein, "Automatic body regulation for maintaining stability of a legged vehicle during rough-terrain locomotion," *IEEE Journal of Robotics and Automation*, vol. 3, pp. 132–141, 1985.

[14] S. Hirose, H. Tsukagoshi, and K. Yoneda, "Normalized energy stability margin: generalized stability criterion for walking vehicles," *Proceedings of the International Conference on Climbing and Walking Robots, Brussels*, 1998.

[15] D. Orin, "Interactive control ofa six-legged vehicle with optimization of both stability and energy," *PhD Thesis, The Ohio State University*, 1976.

[16] Q. Huang and S. Sugano, "Manipulator motion planning for stabilizing a mobile-manipulator," *International Conference on Intelligent Robots and Systems*, vol. 3, 1995.

[17] B.-S. Lin and S.-M. Song, "Dynamic modeling, stability and energy efficiency of a quadrupedal walking machine," *1993 IEEE International Conference on Robotics and Automation, May*, 1993.

[18] E. Garcia and P. G. de Santos, "An improved energy stability margin for walking machines subject to dynamic effects," *Robotica*, vol. 23, p. 1320, 2005.